Advanced Gaussian MRF Rotation-Invariant Texture Features for Classification of Remote Sensing Imagery

Huawu Deng, David A. Clausi
Systems Design Engineering, University of Waterloo, Canada N2L 3G1
h2deng@rousseau.uwaterloo.ca, dclausi@engmail.uwaterloo.ca

Abstract

The features based on Markov random field (MRF) models are usually sensitive to the rotation of image textures. This paper develops an anisotropic circular Gaussian MRF (ACGMRF) model for modelling rotated image textures and retrieving rotation-invariant texture features. To overcome the singularity problem of the least squares estimate (LSE) method, an approximate least squares estimate (ALSE) method is proposed to estimate the parameters of the ACGMRF model. The rotation-invariant features can be obtained from the parameters of the ACGMRF model by the one-dimensional (1-D) discrete Fourier transform (DFT). Significantly improved accuracy can be achieved by applying the rotation-invariant features to classify SAR (synthetic aperture radar) sea ice and Brodatz imagery.

1 Introduction

The development of reliable, robust methods for the consistent classification of SAR (synthetic aperture radar) sea ice imagery has been elusive, even though considerable effort has been made [1]. Tonal features and texture features are two types of features commonly employed to identify sea ice from SAR data. It is indicated [1] that texture features are more suitable than tonal features for describing sea ice image information. Among all kinds of texture features, gray level co-occurrence texture features [2] are commonly used for classification of SAR sea ice imagery. However, this method is restricted since many parameters such as quantization, orientation, displacement, window size, and statistics must be set by the user.

A Markov random field (MRF) model [3] [4] is a powerful tool to model the probability of spatial interactions in an image and has been extensively applied to extract texture features for image classification. The application of MRF models to SAR sea ice classification in the research literature is recognized to be minimal. Given the success of MRF models in other domains, the potential of applying MRF models to classify SAR sea ice imagery should be better explored.

There are a number of signatures of SAR sea ice imagery that can be well represented by MRF models. First, a random nature often exists in all types of sea ice. Second, sea ice shows directional information such as ridges, rubble, rims and deformation due to compression forces [5]. Different sea ice types may have different combinations of directional information in SAR data. The GMRF model is able to describe directional information but the captured directional information is sensitive to image rotation which is a common phenomenon in sea ice imagery. Within the same SAR image, the same sea ice class may show any rotation, depending on the look direction, wind, water current and orientation to coast lines. Due to the rotation of sea ice, directional information captured by the GMRF model is inconsistent and thus leads to a poor performance of classification. Rotation-invariant features based on MRF models should be developed to improve the performance of classifying sea ice.

Some research has considered the frequency domain to extract rotation-invariant features for image textures [6] [7] [8]. Analysis of rotation-invariant features using filters takes advantage of the filters' ability to mimic properties of the human visual system. However, the features obtained through filtering cannot be used to re-generate the original image texture, and filters should be carefully selected for specific image data. Features based on MRF models can be used to re-generate the original texture and take advantage of characterizing random nature in natural images. A new MRF model is therefore developed in this paper to extract rotation-invariant features for texture classification.

The features based on MRF models are generally rotation-variant [8]. Kashyap and Khotanzad [9] constructed an isotropic circular GMRF (ICGMRF) model to extract rotation-invariant features. The ICGMRF model is defined on a circular neighborhood system. The ICGMRF model therefore discards directional information in the possibly non-isotropic textures [8]. To capture directional information, the ICGMRF model will be extended into an anisotropic circular GMRF (ACGMRF) model in this paper.

There is a problem for the ACGMRF model caused by

Proceedings of the 2003 IEEE Computer Society Conference on Computer Vision and Pattern Recognition (CVPR'03)
1063-6919/03 $17.00 © 2003 IEEE

the interpolation of the neighbors which are not on the rectangular grid. As the values of the interpolated neighbors are highly correlated to the values of the nearby pixels which are on the rectangular grid, a singular or nearly singular matrix may occur when using the least squares estimate (LSE) method [10] for parameter estimation. The estimation is unreliable when encountering the singular or nearly singular matrix. This paper proposes an approximate least squares estimate (ALSE) method to overcome the singularity problem. The ALSE method can achieve a very approximate estimation to that provided by the LSE method.

The parameters of the ACGMRF model can then be converted into a set of rotation-invariant features by the one-dimensional discrete Fourier transform (1-D DFT) [11]. The use of the rotation-invariant features based on the ACGMRF model can lead to significant improvement of classifying both Brodatz textures and SAR sea ice imagery, compared with the rotation-variant features based on the GMRF model and the rotation-invariant features based on the ICGMRF model.

2 Anisotropic Circular Gaussian MRF Model

2.1 Isotropic Circular Gaussian MRF (ICGMRF) Model

Three important concepts for MRF models are restated here. Readers are referred to [3] [4] for details of MRF models.

Definition 1 *Let* $S = \{s = (i,j) \mid 1 \le i \le H, 1 \le j \le W,\ i,j,H,W \in I\}$ *be the set of image lattice sites, where* H *and* W *are the image height and width in pixels. A* **neighborhood system** $N = \{N_s, s \in S\}$ *is a collection of subsets of S for which* $s \notin N_s$ *and* $r \in N_s \Leftrightarrow s \in N_r$. N_s *are the neighbors of* s.

In the two-dimensional image lattice S, the pixel values $x = \{x_s | s \in \mathrm{S}\}$ are a realization of random variables $\mathrm{X} = \{X_s | s \in \mathrm{S}\}$.

Definition 2 *A random field X is a* **Markov random field (MRF)** *with respect to the neighborhood system* $N = \{N_s, s \in S\}$ *iff*

1. $P(X = x) > 0$ *for all* $x \in \Omega$*, where* Ω *is the set of all possible* x *on S;*

2. $P(X_s = x_s | X_r = x_r, r \ne s) = P(X_s = x_s | X_r = x_r, r \in N_s)$.

A typical MRF model is the Gaussian MRF (GMRF) model [12] which is widely used for modelling image textures. The GMRF model is also a stationary noncausal 2-dimensional autoregressive process which is described by the following difference equation:

$$x_s = \sum_{s+r \in N_s} \beta_r x_{s+r} + \nu_s, \tag{1}$$

where r is the relative position with respect to the central pixel s, and $\{\nu_s\}$ is a stationary Gaussian noise sequence with zero mean and the autocorrelation given by

$$E(\nu_s \nu_{s+r}) = \begin{cases} \sigma^2 & \text{if } r = (0,0) \\ -\sigma^2 \beta_r & \text{if } r \ne (0,0) \text{ and } s+r \in N_s \\ 0 & \text{otherwise} \end{cases} \tag{2}$$

β_r is the parameter describing directional information between pixels x_{s+r} and x_s. All β_r in the neighborhood system N_s forms the parameter vector $\beta = \{\beta_r | s+r \in N_s\}$.

The property of the neighborhood system N_s is determined by its order and structure. The order of N_s determines the spatial range of the neighborhood. Note that the definition of the order of N_s in [4] is not consistent with the commonly used diagram shown in Fig. 1(a). A modification can be made as follows.

Definition 3 *(modified) A* n**-th order neighborhood system** *is* $N_s^n = \{s+r \mid s+r \in N_s, |r|^2 \le F[n]\}$*, where* $|r|$ *denotes the Euclidian distance between sites* s *and* $s+r$*,* $F[n]$ *is a member of a set of all possible integers in ascending order defined as* $F = \{F[n] \mid F[n] = i^2 + j^2, i, j \in I, i+j > 0, F[k] > F[l]$ *if* $k > l\}$.

The structure of the neighborhood system N_s determines the spatial distribution of neighbors in the neighborhood. For the parameter vector β, its dimensionality and inherent directionality are therefore dependent on the order n together with the structure of the neighborhood system N_s.

A rectangular grid is generally used as the structure of the neighborhood system N_s in a GMRF model [3] [4] [10]. Such a neighborhood system is referred to as a rectangular neighborhood (RN) system in this paper. Fig. 1(a) shows an RN system in different orders. The shape of the RN system changes when it is rotated by any angle except the multiples of $\frac{\pi}{2}$ radians. A rotation of an RN system may therefore generate a different spatial distribution of neighbors with respect to that by the RN system.

Kashyap and Khotanzad [9] proposed for the GMRF model a circular neighborhood (CN) system which can achieve a rotation-invariant spatial distribution of neighbors. All neighbors in a CN system are located on concentric circles. A CN system used by Kashyap and Khotanzad [9] is shown in Fig. 1(b). The values of the neighbors that are not located on the image grid are interpolated by the bilinear interpolation method.

Kashyap and Khotanzad [9] further restricted the parameter β_r to be the same value if $s+r$ is located in the same concentric circle. Eqn. (1) is changed to:

$$x_s = \sum_{k=1}^{n} \beta_k \left[\sum_{|r|=k, s+r \in N_s} x_r \right] + \nu_s, \tag{3}$$

Proceedings of the 2003 IEEE Computer Society Conference on Computer Vision and Pattern Recognition (CVPR'03)
1063-6919/03 $17.00 © 2003 IEEE

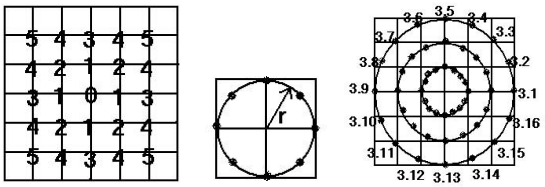

(a) (b) (c)

Figure 1: (a) The fifth-order rectangular neighborhood system. (b) The first-order circular neighborhood system. $r = 1$ is the radius of the circle. (c) The third-order and 16-orientation circular neighborhood system. The number $3.x$ denotes the x-th neighbor on the third concentric circle.

This GMRF model is referred to as an isotropic circular GMRF (ICGMRF) model in this paper.

Although the features based on the parameter $\beta = \{\beta_k, k = 1, ..., n\}$ are rotation-invariant, their limitation of modelling textures is obvious as textures do not necessarily have isotropic neighbors but anisotropic neighbors that can be reflected as directional information [8].

2.2 Anisotropic Circular Gaussian MRF (ACGMRF) Model

Definition 4 *A n-th order circular neighborhood (CN) system is $CN_s^n = \{s + r \mid |r| = k, 0 < k \leq n, k \in I\}$. All neighbors in the same concentric circle are evenly distributed, and the number of neighbors in different circles is the same.*

According to this definition, the CN system used by Kashyap and Khotanzad [9] is the first order CN system CN_s^1. An angle interval between two nearest neighbors in the same concentric circle is defined as $\theta = \frac{2\pi}{\tau}$, where τ is the number of neighbors in one concentric circle in the CN system. The third-order CN system with 16 orientations is shown in Fig. 1(c). It can be seen that a CN_s^3 has a similar spatial distribution of neighbors as the ninth-order RN system.

The GMRF model defined in the n-th order CN system CN_s^n has the following difference equation:

$$x_s = \sum_{s+r \in CN_s^n} \beta_r \, x_{s+r} + \nu_s \,, \tag{4}$$

As the parameter β_r may be different for different circular neighbors, this model is referred to as an **anisotropic circular GMRF (ACGMRF) model**.

3 Parameter Estimation

3.1 Approximate Least Squares Estimate

Due to its computation efficiency, the least squares estimate (LSE) method has been commonly accepted to estimate the parameters of GMRF models [10]. Define a quadratic difference Q between the central pixel x_s and its neighbors in the ACGMRF model:

$$Q = \sum_s \left(x_s - \sum_{s+r \in CN_s^n} \beta_r \, x_{s+r} \right)^2 . \tag{5}$$

The least squares estimate of β_r is [10]:

$$\beta = \left[\sum_s Z_s Z_s^T \right]^{-1} \left[\sum_s Z_s x_s \right] , \tag{6}$$

where $Z_s = col\{x_{s+r} \mid s + r \in CN_s^n\}$.

However, the above solution may encounter a singularity problem when $\tau \times n$ is larger than the number of neighbors in the rectangular grid. This is because the interpolated values of the neighbors that are not located on the grid are highly correlated to the values of the neighbors that are located on the grid. The estimate is unreliable when encountering a singular or near singular matrix. Using uncorrelated data can overcome the singularity problem. For this purpose, the parameters of the ACGMRF model can be divided into a number of groups and then estimated separately.

Denote the set of all parameters of the n-th order ACGMRF model by $\beta = \{\beta_r \mid s + r \in CN_s^n, \forall s\}$. β can be divided into m groups: $\beta^1, \beta^2, \cdots, \beta^m$. Each group β^k describes a corresponding group of neighbors in CN_s^n, denoted by $(CN_s^n)^k$. The parameter groups $\beta^1, \beta^2, \cdots, \beta^m$ should satisfy the following conditions:

1. $\beta^k = \{\beta_r^k \mid \beta_r^k = \beta_r, s+r \in (CN_s^n)^k\}$, *where* $1 \leq k \leq m$ *and* $k \in I$.
2. $\beta^k \neq \emptyset$ *and* $\beta^k \bigcap \beta^{k'} = \emptyset$, *for* $1 \leq k, k' \leq m$ *and* $k \neq k'$.
3. $\beta^1 \bigcup \beta^2 \bigcup \cdots \bigcup \beta^m = \beta$.

The groups of pixel values $x_{CN_s^n} = \{x_{s+r} | s + r \in CN_s^n\}$ corresponding to $\beta^1, \beta^2, \cdots, \beta^m$ are denoted by $x_{CN_s^n}^1, x_{CN_s^n}^2, \cdots, x_{CN_s^n}^m$, where $x_{CN_s^n}^k = \{x_{s+r}^k \mid x_{s+r}^k = x_{s+r}, s + r \in (CN_s^n)^k\}$.

Based on taking partial derivative of the quadratic difference Q (for succinctness, the details are not shown), two approximate leat squares estimation method can be obtained.

The first approximate least squares estimate (ALSE) method can be designed as:

$$\beta^k = \left[\sum_s Z_s^k (Z_s^k)^T \right]^{-1} \left[\sum_s Z_s^k x_s \right] , \tag{7}$$

where $Z_s^k = col\{x_{s+r} \mid s+r \in (CN_s^n)^k\}$ and $1 \leq k \leq m$.

The second approximate least squares estimate (ALSE) method can be designed as:

Proceedings of the 2003 IEEE Computer Society Conference on Computer Vision and Pattern Recognition (CVPR'03)
1063-6919/03 $17.00 © 2003 IEEE

1. For estimating the first group of parameters β^1,

$$\beta^1 = \left[\sum_s Z_s^1 (Z_s^1)^T\right]^{-1} \left[\sum_s Z_s^1 x_s\right]. \quad (8)$$

2. For estimating the k-th group of parameters β^k, where $1 < k \leq m$,

$$\beta^k = \left[\sum_s Z_s^k (Z_s^k)^T\right]^{-1} \left[\sum_s Z_s^k (x'_s + x_s)\right], \quad (9)$$

where $x'_s = \sum_{k'=1}^{k-1} (\frac{1}{m} x_s - \sum_{\beta^{k'}} \beta_r^{k'} x_{s+r}^{k'})$.

Experimental results indicate that the second ALSE method has a more approximate least squares estimate than the first ALSE method. The second ALSE method is therefore used for the experiments in this paper. The following rules are adopted in this paper to divide the parameters of the ACGMRF model into different groups for the ALSE method.

1. *The parameters for the neighbors on different concentric circles should be divided into different groups.*
2. *A basic number of parameters for the n-th concentric circle is set to the number of pixels on the border of the nearest rectangular grid. When the number of parameters on the n-th concentric circle exceeds the basic number of the n-th concentric circle, these parameters should be separated into different groups.*
3. *The angle intervals θ between the nearest neighbors in a group should be the same.*
4. *The parameters on a lower-order concentric circle should be estimated before those on a higher-order concentric circle.*

3.2 Rotation-Invariant Features

The parameters of the ACGMRF model form a one-dimensional (1-D) vector by an order of each parameter regarding its location in the CN system (see Fig. 1(c)). A rotation of the circular neighborhood is therefore equivalent to shifting the 1-D parameter vector [11]. The 1-D discrete Fourier transform (1-D DFT) can be applied to the 1-D parameter vector and obtain a magnitude vector of the DFT coefficients. The magnitude vector corresponding to a shifted vector remains unchanged with respect to the magnitude vector corresponding to the original vector. The magnitude vector corresponding to the 1-D parameter vector is therefore a set of rotation-invariant features. Note that the number of non-zero and non-redundant components in the magnitude vector is much smaller than the total dimensions of the magnitude vector. For a symmetric ACGMRF model (which is implemented in experiments of this paper), the number of non-zero and non-redundant components of the magnitude vector is not greater than $\frac{n \times \tau}{4} + 1$, as the values of the 1-D parameter vector are real and symmetric.

4 Experimental Results

4.1 Synthesis of Rotated Image Textures

There are two objectives for this texture synthesis experiment. One is to verify that the ALSE method is able to estimate the parameters of the ACGMRF model. Another is to verify that a rotation of the circular neighborhood system, which corresponds to a shift of the parameter vector, will accordingly generate a rotated image texture.

The raffia texture (D084) in the Brodatz database [13] is selected as the original texture. The ALSE method is used to estimate a set of parameters of the third-order and 16-orientation ACGMRF model. Five angles (0, $\frac{\pi}{8}$, $\frac{\pi}{4}$, $\frac{3\pi}{8}$ and $\frac{\pi}{2}$ radians) are used to rotate the circular neighborhood system in the counterclockwise direction, and five sets of shifted parameter vectors for each rotated texture are generated accordingly. The Metropolis sampling method [4] is employed for texture synthesis. The results are shown in Fig. 2.

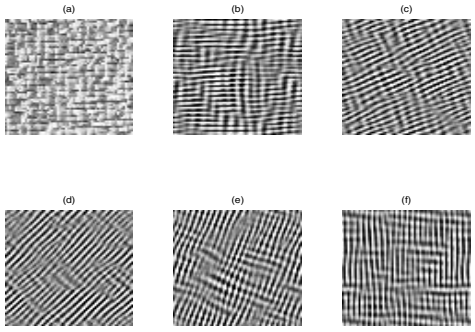

Figure 2: Texture synthesis based on the ACGMRF model by rotating its CN system. (a) Original texture (D084); (b)-(f) are synthesized textures with the parameters rotated 0, $\frac{\pi}{8}$, $\frac{\pi}{4}$, $\frac{3\pi}{8}$, and $\frac{\pi}{2}$ radians respectively.

Fig. 2(b) shows both horizontal and vertical directional information similar with that in the original texture (Fig. 2(a)). Figs. 2(c), (d), (e) and (f) are the synthesized textures using the parameters whose circular neighborhood system is rotated $\frac{\pi}{8}$, $\frac{\pi}{4}$, $\frac{3\pi}{8}$ and $\frac{\pi}{2}$ radians respectively. These textures display the corresponding rotated directional information with respect to the original texture.

4.2 Classification Methodology

A supervised classification scheme is employed for the classification experiments in this paper. First, all image texture samples are separated into two sets: one set for training, another set for testing. Second, a set of rotation-invariant features based on the ACGMRF model is extracted from each image texture sample, denoted by $f_j = \{f_{jk} | 1 \leq k \leq$

Proceedings of the 2003 IEEE Computer Society Conference on Computer Vision and Pattern Recognition (CVPR'03)
1063-6919/03 $17.00 © 2003 IEEE

$\frac{\tau \times n}{4} + 1\}$ for the j-th sample. Third, the mean of the training sets of rotation-invariant features of each texture class is used to represent the feature of the texture class, denoted by $\mu_i = \{\mu_{ik} = \frac{1}{\dim(f^i)} \sum_{f_j \in f^i} f_{jk} \mid 1 \le k \le \frac{\tau \times n}{4} + 1\}$ for the i-th texture class whose feature set is f^i; Fourth, the distance proposed in [9] is used in this paper as the metric to measure the difference between two textures:

$$\hat{i} = \arg_i \min \{D(f_j, \mu_i), i = 1, 2, \cdots, n\}, \tag{10}$$

where $D(f_j, \mu_i) = \sum_{k=1}^{\frac{\tau \times n}{4}+1} \left| \frac{f_{jk} - \mu_{ik}}{\sigma_k} \right|$, and $\sigma_k = std\{f_{jk}, \text{ for all } j\}$ is the standard deviation of the k-th rotation-invariant feature component over the entire training data and functions as a normalization constant.

An error matrix is produced when classifying the test data. Kappa (κ) coefficients and associated confidence intervals (σ) are commonly used to evaluate each error matrix [14]. When two error matrices are compared, the following test statistic can be used to determine a significance value (using a significance level of 5%):

$$Z \sim \frac{\kappa_1 - \kappa_2}{\sqrt{\sigma_1^2 + \sigma_2^2}}, \tag{11}$$

where the κ coefficient is defined as $\kappa = \frac{N \sum_{i=1}^{M} X_{ii} - \sum_{i=1}^{M} X_{i+} X_{+i}}{N^2 - \sum_{i=1}^{M} X_{i+} X_{+i}}$, where M is the number of classes, X_{ii} is the ith value on the error matrix diagonal; X_{i+} and X_{+i} are the marginal sums of rows and columns respectively, and N is the total number of samples.

4.3 Classification of Brodatz Textures

The imagery of Brodatz textures [13] is commonly used as a set of test data for the generic texture interpretation research. Each Brodatz sample is assumed to contain only one class, however, this cannot be guaranteed for remote sensing data. Twelve Brodatz textures are selected for classification. Each Brodatz texture has 256×256 pixels. These Brodatz textures include regular textures, i.e. D006 (wire), D011 (woolen cloth), D019 (woven cloth), D021 (French canvas), D052 (oriental shaw cloth), D079 (oriented grass-fiber cloth), D095 (brick wall) and non-regular textures, i.e. D029 (sand), D036 (lizard skin), D037 (water), D084 (raffia), D087 (fossilized sea fan).

Twelve rotated images are generated from each texture by rotating the texture with twelve angles (0, $\frac{\pi}{12}$, $\frac{\pi}{6}$, $\frac{\pi}{4}$, $\frac{\pi}{3}$, $\frac{5\pi}{12}$, $\frac{\pi}{2}$, $\frac{7\pi}{12}$, $\frac{2\pi}{3}$, $\frac{3\pi}{4}$, $\frac{5\pi}{6}$ and $\frac{11\pi}{12}$ radians). Only the central 128×128 regions in the twelve rotated images are used to comprise the data set for classification. Each 128×128 rotated image is further segmented into sixteen 32×32 non-overlapped subimages as the basic texture samples to be classified. Then a set of rotation-invariant features is extracted from each subimage modelled by the third-order and 24-orientation ACGMRF model. By the classification scheme in Eqn. (10), the testing subimages will be classified into one of the twelve texture classes.

Table 1: Classification accuracy rates (%) over twelve Brodatz textures by the features of the ACGMRF model, the GMRF model and the ICGMRF model. Each class of texture has 192 samples.

Texture Name	ACGMRF	GMRF	ICGMRF
D006	82.29	37.50	77.08
D011	81.25	42.71	56.25
D019	87.50	44.79	54.17
D021	81.25	31.25	61.46
D029	75.00	34.38	55.21
D036	84.38	13.54	44.79
D037	88.54	22.92	34.38
D052	78.13	48.96	37.50
D079	82.29	12.50	53.15
D084	73.96	09.38	54.17
D087	82.29	36.46	44.79
D095	88.54	11.46	65.63
Average	82.12	28.82	53.21

Table 2: Kappa coefficients (κ) and associated confidence intervals (σ) for the classification of twelve Brodatz textures by the features of the ACGMRF model, the GMRF model and the ICGMRF model.

	ACGMRF	GMRF	ICGMRF
κ	0.7992	0.1916	0.5244
σ	0.0094	0.0106	0.0121

Comparative experiments are conducted by using the fourth-order GMRF features (the determination of the order of a GMRF model is based on the method in [10]) and the third-order ICGMRF model features. The result shows that the classification accuracy rate by the rotation-invariant features of the ACGMRF model is improved about 30 percentage points with respect to that by the features of the third-order ICGMRF model and more than 50 percentage points with respect to that by the features of the fourth-order GMRF model. The classification accuracy rates by these methods are listed in Table 1. The significant improvement of classification accuracy by the ACGMRF model with respect to the ICGMRF/GMRF model is also demonstrated by the statistic test of the data in Table 2.

4.4 Classification of SAR Sea Ice Imagery

This experiment uses two scenes of C-band HH Radarsat ScanSAR data covering the Gulf of St. Lawrence. One scene was captured on February 19th, 1997; another scene was captured on February 12th, 1999. The incidence angles are between 20 and 49 degrees when capturing both scenes and the pixel spacing is $100m$.

The images of different ice types are extracted from the two scenes. Here, each image should contain only one ice type or at least one ice type dominating the image region. A total of 20 images are extracted to contain new ice and first-year ice. Each image is further segmented into a number of 32×32 non-overlapped subimages as the basic ice samples

Proceedings of the 2003 IEEE Computer Society Conference on Computer Vision and Pattern Recognition (CVPR'03)
1063-6919/03 $17.00 © 2003 IEEE

Table 3: Classification rates (%) over SAR data by the features of the ACGMRF model, the GMRF model and the ICGMRF model.

Ice Type	Samples	ACGMRF	GMRF	ICGMRF
New ice	398	95.22	58.81	55.82
First-year ice	440	85.41	77.57	77.03

Table 4: Kappa coefficients (κ) and associated confidence intervals (σ) for the classification of SAR data by the features of the ACGMRF model, the GMRF model and the ICGMRF model.

	ACGMRF	GMRF	ICGMRF
κ	0.8020	0.3666	0.3314
σ	0.0225	0.0353	0.0358

to be classified. A total of 398 new ice samples and 440 first-year ice samples comprise the test data.

The third-order and 24-orientation ACGMRF model, the fourth-order GMRF model and the third-order ICGMRF model are applied to these ice samples to extract three sets of texture features. The classification results based on these features are listed in Table 3. The classification accuracy rate of the new ice by the ACGMRF model is improved more than 30 percentage points with respect to those by the GMRF model and the ICGMRF model. One reason is that strong directional information exists in the new ice samples; another reason is that the new ice images have randomly rotated positions mostly due to the water current and the pressure from nearby land or other ices. There are about 8 percentage points improved by the ACGMRF model for the first-year ice with respect to the GMRF model. This moderate improvement is rational since the first-year ice images do not show strong directional information but much stronger random information. The significant improvement of classification accuracy by the ACGMRF model with respect to the ICGMRF/GMRF model is also demonstrated by the statistic test of the data in Table 4.

5 Conclusion

An anisotropic circular GMRF (ACGMRF) model is developed by extending the isotropic circular GMRF (ICGMRF) model to model the textures with directional information. To overcome the singularity problem for the least squares estimate method, an approximate least squares estimate method is proposed in the paper. By using the one-dimensional DFT, the parameters of the ACGMRF model can be converted into a set of rotation-invariant features. Experimental results indicate that a significant improvement of classification accuracy is achieved by the ACGMRF model with respect to the ICGMRF model or the GMRF model.

Acknowledgements

The authors thank GEOIDE (Geomatics for Informed Decision) and CRYSYS (Cryosphere System in Canada) for financial support of this project and CIS (Canadian Ice Services) for providing the SAR data.

References

[1] L. K. Soh and C. Tsatsoulis, "Texture Analysis of SAR Sea Ice Imagery Using Gray Level Co-occurrence Matrices," *IEEE Trans. Geoscience and Remote Sensing*, vol. 37, no. 2, pp. 780–795, 1999.

[2] R. M. Haralick, K. Shanmugam, and I. Dinstein, "Textural Features for Image Classification," *IEEE Trans. Sys. Man Cybern*, vol. 3, pp. 610–621, 1973.

[3] J. E. Besag, "Spatial Interaction and the Statistical Analysis of Lattice Systems (with Discussion)," *J. Royal Stat. Soc.*, vol. B-36, pp. 192–236, 1974.

[4] S. Z. Li, *Markov Random Field Modeling in Computer Vision*, New York: Springer-Verlag, 1995.

[5] M. E. Shokr, "Evaluation of Second-Order Texture Parameters for Sea Ice Classification from Radar Images," *J. Geophysical Research*, vol. 96, no. C6, pp. 10 625–10 640, 1991.

[6] R. Porter and N. Canagarajah, "Robust Rotation-Invariant Texture Classification: Wavelet, Gabor Filter and GMRF Based Schemes," *IEE Proc. - Vis. Image Signal Process*, vol. 144, no. 3, pp. 180–188, 1997.

[7] G. M. Haley and B. S. Manjunath, "Rotation-Invariant Texture Classification Using A Complete Space-Frequency Model," *IEEE Trans. Image Processing*, vol. 8, no. 2, pp. 255–269, 1999.

[8] F. S. Cohen, Z. G. Fan, and M. A. Patel, "Classification of Rotated and Scaled Textured Images Using Gaussian Markov Random Field Models," *IEEE Trans. Pattern Anal. Machine Intell.*, vol. 13, no. 2, pp. 192–202, 1991.

[9] R. L. Kashyap and A. Khotanzad, "A Model-Based Method for Rotation Invariant Texture Classification," *IEEE Trans. Pattern Anal. Machine Intell.*, vol. 8, no. 7, pp. 472–481, 1986.

[10] R. L. Kashyap and R. Chellapa, "Estimation and Choice of Neighbors in Spatial-Interaction Models of Images," *IEEE Trans. Information Theory*, vol. 29, no. 1, pp. 60–72, 1983.

[11] H. Arof and F. Deravi, "Circular Neighborhood and 1-D DFT Features for Texture Classification and Segmentation," *IEE Proc. - Vis. Image Signal Process*, vol. 145, no. 3, pp. 167–172, 1998.

[12] S. Geman and D. Geman, "Stochastic Relaxation, Gibbs Distributions, and the Bayesian Restoration of Images," *IEEE Trans. Pattern Anal. Machine Intell.*, vol. 6, no. 6, pp. 721–741, 1984.

[13] P. Brodatz, *Texture–A Photographic Album for Artists and Designers*, Reinhold, New York, USA, 1968.

[14] T. Bishop, S. Fienberg, and P. Holland, *Discrete Multivariate Analysis - Theory and Practice*, Cambridge, Mass.: MIT Press, 1975.

Proceedings of the 2003 IEEE Computer Society Conference on Computer Vision and Pattern Recognition (CVPR'03)
1063-6919/03 $17.00 © 2003 IEEE